

Antibacterial and anticancerous drug loading kinetics for (10-x) CuO-xZnO-20CaO-60SiO₂-10P₂O₅ (2 ≤ x ≤ 8) mesoporous bioactive glasses

Shikha Garg¹ · Swati Thakur¹ · Aayush Gupta² · Gurbinder Kaur² · Om Prakash Pandey²

Received: 9 September 2016 / Accepted: 29 November 2016 / Published online: 9 December 2016
© Springer Science+Business Media New York 2016

Abstract In the present study, antibacterial and anticancerous drug loading kinetics for the (10-x)CuO-xZnO-20CaO-60SiO₂-10P₂O₅ (2 ≤ x ≤ 8, varying in steps of 2) mesoporous bioactive glasses (MBGs) have been studied. XRD analysis of the as prepared glass samples proved its amorphous nature. Scanning electron microscopy (SEM) revealed the apatite layer formation on the surface of the MBGs after soaking for 15 days in SBF. Ion dissolution studies of calcium, phosphorous and silicon have been performed using inductively coupled plasma (ICP). FTIR and Raman analysis depicted about the presence of various

bonds and groups present in the glasses. The pore size of MBGs lies in the range of 4.2–9.7 nm. Apart from this, specific surface area of the MBGs varied from 263 to 402 cm²/g. The MBGs were loaded with Doxorubicin (DOX), Vancomycin (VANCO) and Tetracycline (TETRA) drugs among which, the decreasing copper content influenced the loading properties of doxorubicin and tetracycline drugs. Vancomycin was fully loaded almost in all the MBGs, whereas other drugs depicted varying loading with respect to the copper content.

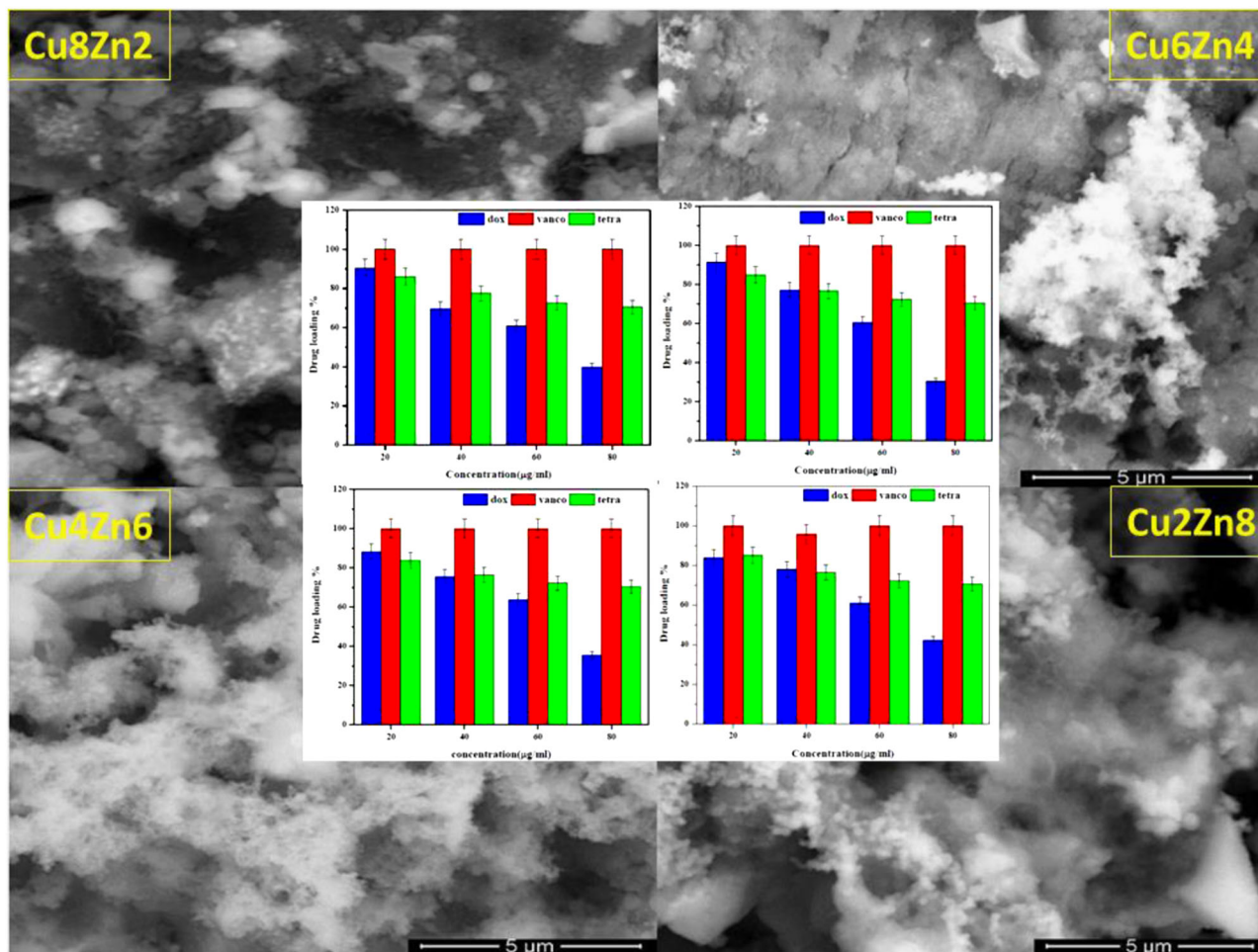
✉ Gurbinder Kaur
gkapds@gmail.com

✉ Om Prakash Pandey
oppandey@thapar.edu

¹ Department of Physics, Punjabi University, Patiala 147002, India

² School of Physics and Materials Science, Thapar University, Patiala 147004, India

Graphical Abstract



1 Introduction

Many research groups have been working on the targeted drug delivery aspect for the treatment of defected areas especially tumor cancer sites in a patient's body. Recently, researchers are trying to accomplish this target with the help of mesoporous bioactive glasses (MBGs). MBGs show enhanced properties due to which, these are considered as potential candidates for the targeted drug delivery. These glasses can reveal wide change in properties even with little tailoring in the chemical composition [1, 2]. Many research groups have been working on the fabrication of MBGs and analyzing their properties [3–9]. Addition of structure directing agent like cetyltrimethyl ammonium bromide (CTAB), P123 and F127 into the glass structure result in the formation of MBGs. The great drug loading efficiency of MBGs is due to their mesochannels. The drug to be delivered is entrapped in the channels of the mesoporous glass and thereby released at the targeted site [10–14]. Recent work done by Hum et al. [5] showed that bioactive glasses

have the potential to induce angiogenesis along with influencing gene effect [5, 15–18]. Unique features like biocompatibility, biodegradability, osteoconductivity makes MBGs an excellent drug delivery vehicle [5, 19–22]. Drug loaded MBGs release conductive factors enhancing osteogenesis, bone regeneration and proliferation [8]. Regi et al. [15] worked on the controlled drug delivery system with mesoporous material MCM-41 as promising drug carrier [15–20]. The mesoporous silica had some unique features like high pore volume, high surface area, ordered pore network and silanol-containing surface making it considerable choice for controlled drug delivery. The drug may get released prematurely due to premature degradation, so it is important to control the release kinetics of drug to avoid any side effects [23–28]. MBGs can also be used for treating the orthopedic problems. Artificial bone substitutes can be fabricated using MBGs, e.g. bioactive porous scaffolds, which can be further used to repair the damaged bone [28–34]. However, only 45S5 Bioglass[®] and silicate glasses have been proposed for the fabrication of scaffolds using

different techniques [35]. The drug, which is to be delivered to the defect site in a patient's body, is injected in the pores of the scaffold and further, scaffold is implanted onto the defect site. Bioactive scaffolds have the ability to degrade and subsequently release the drug on the defected site. According to Wu et al. [36], combination of scaffolds with angiogenic (for inducing vascularisation), osteoconductive (for guidance of new bone growth) and osteostimulative factors (for promoting new bone formation) can greatly enhance the regeneration of large bone defects [36–41]. Even though powerful drugs are being introduced for healing fatal diseases in today's era, however all these drugs have toxic effects on the normal tissues [42].

Hence, in the present investigation, we have synthesized $(10-x)\text{CuO}-x\text{ZnO}-20\text{CaO}-10\text{P}_2\text{O}_5-60\text{SiO}_2$, (where $2 \leq x \leq 8$) MBGs with varying zinc and copper content. Copper and zinc are important nutrients for human body as zinc plays a role in immune function, protein synthesis, wound healing, cell division and DNA synthesis, whereas, copper plays predominant part in metabolism [43–46]. Variation of zinc and copper content on the drug loading efficiency of bioactive glasses is investigated in the present study. The drugs, doxorubicin (DOX), vancomycin (VANCO) and tetracycline (TETRA) were used to investigate the loading efficiency of MBGs. DOX is an anti-tumor drug, whereas, VANCO and TETRA are the antibacterial drugs. The nature of the glass was analyzed with X-ray diffractometer. The various bands and groups present in the MBGs were analyzed using Fourier transform infrared spectroscopy (FT-IR) and Raman spectroscopy. The density, pore size and magnetic characteristics of the respective glasses have also been analyzed.

2 Experimental techniques

The mesoporous bioactive glasses (MBGs) with composition $(10-x)\text{CuO}-x\text{ZnO}-60\text{SiO}_2-10\text{P}_2\text{O}_5-20\text{CaO}$ ($2 \leq x \leq 8$) was prepared using sol-gel technique with cetyltrimethyl ammonium bromide (CTAB) as a structure directing agent. The raw materials used for the fabrication of glasses were tetraethylorthosilane TEOS ($\geq 99\%$, purity Sigma-Aldrich), triethyl phosphate TEP ($\geq 98\%$, purity Sigma-Aldrich), calcium nitrate tetrahydrate ($\text{Ca}(\text{NO}_3)_2 \cdot 4\text{H}_2\text{O}$, extra pure Sigma-Aldrich), zinc nitrate hexahydrate ($\text{Zn}(\text{NO}_3)_2 \cdot 6\text{H}_2\text{O}$, $\geq 99\%$ purity, Sigma-Aldrich) and cupric nitrate trihydrate ($\text{Cu}(\text{NO}_3)_2 \cdot 3\text{H}_2\text{O}$, extra pure Sigma-Aldrich).

The composition of as prepared glasses is listed in Table 1. 1.5 g CTAB was dissolved in 25 ml of ethanol by violent stirring. For preparing $8\text{Cu}_2\text{Zn}$ sample, 0.512 ml of triethyl phosphate (TEP) was added to 2.01 ml of tetraethylorthosilane (TEOS) with constant stirring. 1 M of HNO_3 was used as a catalyst for the hydrolysis of TEOS + TEP mixture. Molar ratio kept here was HNO_3+

Table 1 Composition of mesoporous bioactive glasses (MBGs) (mol%)

Sample name	CuO	ZnO	SiO ₂	P ₂ O ₅	CaO
Cu8Zn2	8	2	60	10	20
Cu6Zn4	6	4	60	10	20
Cu4Zn6	4	6	60	10	20
Cu2Zn8	2	8	60	10	20

deionized water:TEOS + TEP = 8:1. The solution was stirred for 1 h. Thereafter, 0.713 g of calcium nitrate tetrahydrate, 0.087 g of zinc nitrate hexahydrate and 0.297 g of cupric nitrate trihydrate were added after each other at an interval of 30 min with continuous stirring. After this, the ethanol and CTAB containing mixture was added to the as prepared mixture and was stirred for 2 h and sol was prepared. The as prepared sol was then kept in Petri dish for the evaporation induced self assembly (EISA) process. Following this, the dried gel was kept at 70° for 2 days for complete drying.

The nature of glass was analyzed using high resolution XRD in an X'Pert PRO MPD diffractometer with the scanning speed of 2°min^{-1} for angular range between 10 to 70°. Furthermore, the density of glasses was measured applying Archimedes principle with distilled water as buoyant. To measure pore size, pore volume and specific surface area of the glasses, BET analysis with N₂ gas adsorption-desorption isotherm (Gemini V analyzer, Germany) was done. Before every measurement, reduced pressure was used to degas the samples for 15 h at 200 °C.

Simulated body fluids (SBF) solution was prepared using the required ion concentrations [8, 47]. The pellets of glass of 1 cm (diameter) were made using hydraulic press. Glass pellets were dipped in SBF solution kept in clean glass bottles. The bottles were tightly covered and kept in water bath at 37 °C. After soaking process, the samples were washed with deionized water. The apatite layer formation was determined by environmental SEM. Scanning electron measurements were recorded with SEM (FEI Quanta 600 FEG, Hillsboro) with ET detector and low pressure of 1 Torr under hydrated conditions. The ion dissolution studies were performed by inductively coupled plasma (ICP-OES) spectroscopy. Glass pellets were immersed in 50 ml SBF at 37 °C up to 120 h. Extracts were obtained via filtration (1 μm) at 12, 24, 36, 48, 72, 96, 120 and then analyzed by ICP. For the ICP measurements, PerkinElmer Optima 7000 DV ICP-OES instrument (PerkinElmer, Inc., Shelton, CT, USA) equipped with WinLab32, Version 4.0 software was used. For observing vibrational, rotational and other low-frequency modes in a system, Raman spectroscopy is used. The samples were characterized by Labram HR 800

Evo Raman Spectrometer with He–Cd laser. To analyze the bonding of samples, fourier transform infra-red (FT-IR) spectroscopy is used. Over a wide spectral range (400–4000 cm^{-1}), high spectral resolution data is collected by FT-IR spectrometer (Model: Agilent Resolution Pro (cary 660)). To prepare the pellets for analyzing the behavior of sample, MBGs were mixed with KBr. The ratio of sample: KBr is 1:100.

For the drug loading, vancomycin hydrochloride, doxorubicin hydrochloride and tetracycline drugs were used into the mesoporous channels of the glasses. For loading of the drugs, doxorubicin (DOX), vancomycin (VANCO) and tetracycline (TETRA) were firstly dissolved in double distilled water (ddH₂O) with concentrations of 20, 40, 60 and 80 $\mu\text{g/ml}$. 50 mg of each MBG was then dissolved in 4 ml of DOX–ddH₂O, VANCO–ddH₂O and TETRA–ddH₂O solution, followed by shaking at room temperature for 24 h. To separate the MBG and supernatant, after shaking, all the samples were centrifuged at 2000 rpm for 15 min. To determine the loading efficiency of the MBGs, the DOX, VANCO and TETRA concentration difference in the loading medium was calculated before and after loading using UV analysis. The drug loading of the mesoporous glasses were recorded at room temperature with distilled water as reference using a double beam UV-VIS spectrophotometer (Model: Hitachi 3900H) in the wavelength range of 200–800 nm. The magnetic behavior of the MBGs, was analyzed with vibrating sample magnetometer (VSM) (Lake Shore 7404). The spectral range taken to analyze the particle was ± 1 Tesla along with the step size of 500 Oe.

3 Results

3.1 XRD and physical parameters

XRD pattern indicates the amorphous nature of glass as shown in Fig. 1. As Bragg's diffraction peaks are absent, hence the absence of crystalline phases is also confirmed Density (ρ) of samples was calculated using following equation:

$$V_m = \frac{M}{\rho} \quad (1)$$

where M is the molar mass and V_m is the molar volume of the glasses. Molar mass of the as prepared samples lies between 66.15 and 66.30 g/mol. The values of molar mass, molar volume and density are listed in Table 2.

3.2 BET analysis

The values of pore size, pore volume and specific surface area for MBGs are listed in Table 3. With the increase of the

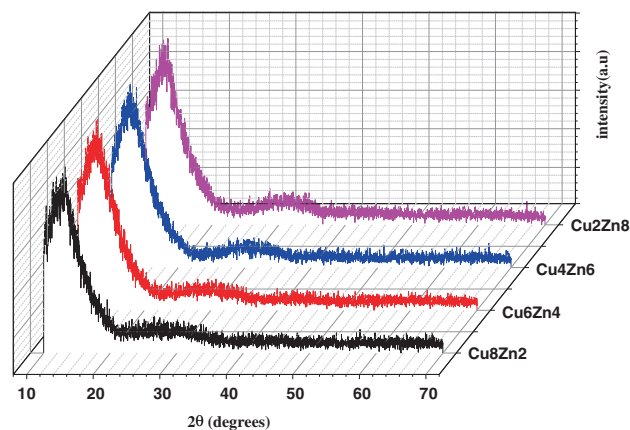


Fig. 1 XRD pattern of as prepared glasses

Table 2 Molar mass, molar volume and density of glasses

Sample name	Molar mass (M) (g/mol)	Molar volume (V_m) (cm^3/mol)	Density (g/cm^3)
Cu8Zn2	66.18	46.61	1.41
Cu6Zn4	66.23	38.73	1.71
Cu4Zn6	66.26	38.53	1.72
Cu2Zn8	66.30	46.02	1.44

zinc content in the MBGs, the pore size increased from 4 to 10 nm, approximately.

3.3 Apatite layer formation

The SEM micrographs for Cu8Zn2, Cu6Zn4, Cu4Zn6 and Cu2Zn8 MBGs after soaking for 15 days in SBF are shown in Fig. 2a–d. All the MBGs show apatite layer formation on their surface.

3.4 ICP analysis

Figure 3a–c shows the dissolution profiles for calcium (Ca), phosphorous (P) and silicon (Si) respectively, for all the MBGs when soaked in the SBF as a function of time. It is asserted from Fig. 3a that for all MBGs, Ca concentration increases sharply up to 12 h of soaking in the SBF solution. However, P does not show any increasing or decreasing trend upto 48 h of soaking in SBF solution (Fig. 3b). However, rapid increase in concentration of Si up to 12 h of soaking in SBF can be seen for all the MBGs (Fig. 3c).

3.5 Raman spectroscopy

Raman spectra show different bands and peaks of different components of glass sample as depicted in Fig. 4.

Silica component is abundant for all the MBGs, so the most prominent peaks belong to silica. For $450\text{--}550\text{ cm}^{-1}$ region, phosphate and silica Si-O_b-Si peaks are observed [48–50]. Prominent phosphate peaks are observed within $550\text{--}600\text{ cm}^{-1}$ range, for glass sample Cu8Zn2. The peak obtained in $800\text{--}950\text{ cm}^{-1}$ range represents the presence of phosphate P-O-P component. Peak observed for $1400\text{--}1550\text{ cm}^{-1}$ is due to the presence of H₂O molecule.

3.6 FT-IR

FT-IR spectra for the as prepared glass samples is observed and is shown in Fig. 5. All the glass samples showed similar peak positions as listed in Table 4. Due to the presence of high silica component in the glasses, silicate bands were prominent.

3.7 Loading kinetics

Three drugs i.e. vancomycin hydrochloride (VANCO), doxorubicin hydrochloride (DOX) and tetracycline (TETRA) have been loaded here in different glass samples as demonstrated

below. The calibration curves of different drugs VANCO, DOX and TETRA are shown in Fig. 6a–c respectively, at different concentrations. These calibration curves help in determining the loading of drugs. Slope of these curves is found and then by knowing the unloaded drug values, amount of loaded drug can be calculated. The following equations, give the slopes of VANCO, DOX and TETRA drugs.

$$\text{Slope of VANCO} - Y = 0.003x + 0.035, R^2 = 0.955 \quad (2)$$

$$\text{Slope of DOX} - Y = 0.001x + 0.015, R^2 = 0.982 \quad (3)$$

$$\text{Slope of TETRA} - Y = 0.030x + 0.036, R^2 = 0.999 \quad (4)$$

Table 3 Pore size, pore volume and surface area of as prepared glass samples

Sample name	Pore volume (cm ³ /g)	Surface area (cm ² /g)	Pore size (nm)
Cu8Zn2	0.77	263	4.2
Cu6Zn4	0.79	318	6.3
Cu4Zn6	0.93	395	8.5
Cu2Zn8	0.86	402	9.7

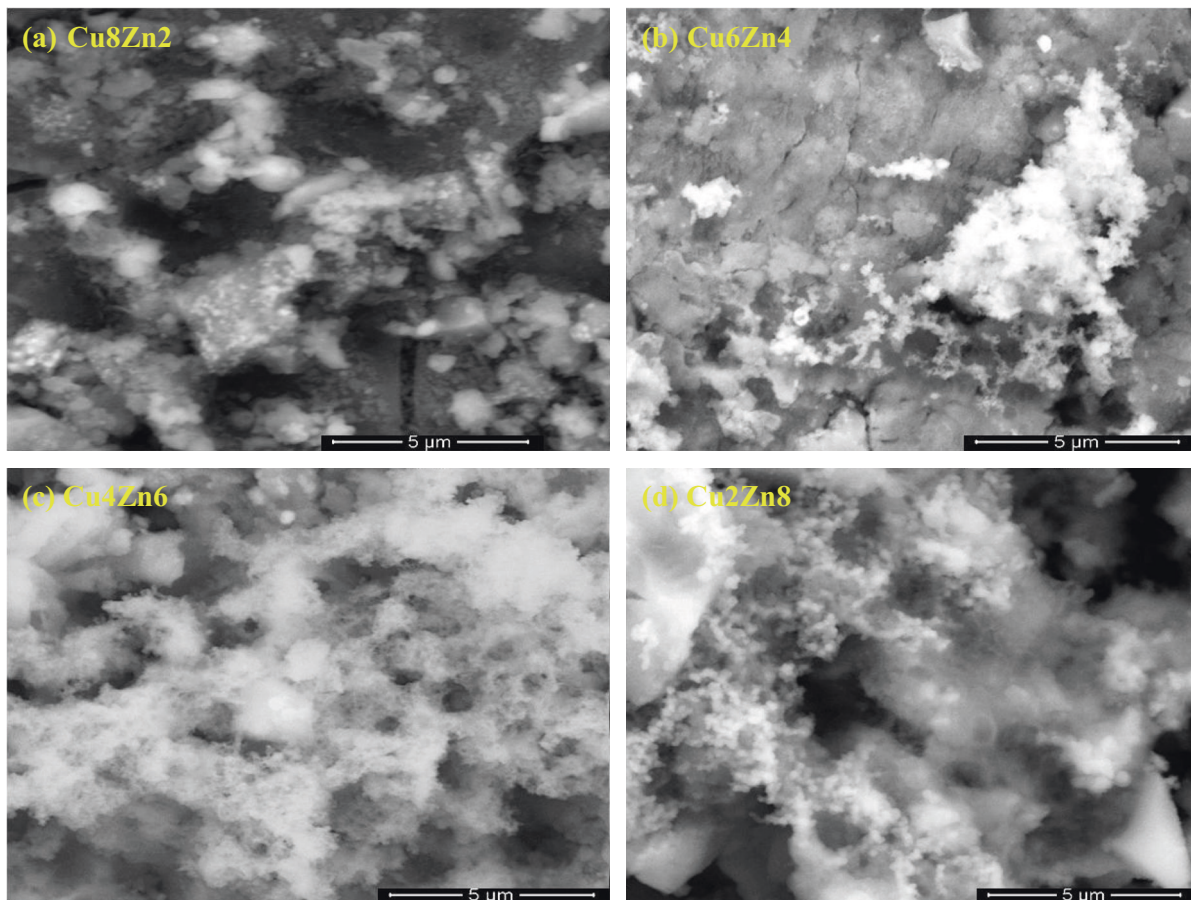


Fig. 2 The apatite formation for a Cu8Zn2, b Cu6Zn4, c Cu4Zn6 and d Cu2Zn8 samples after soaking in SBF solution for 15 days

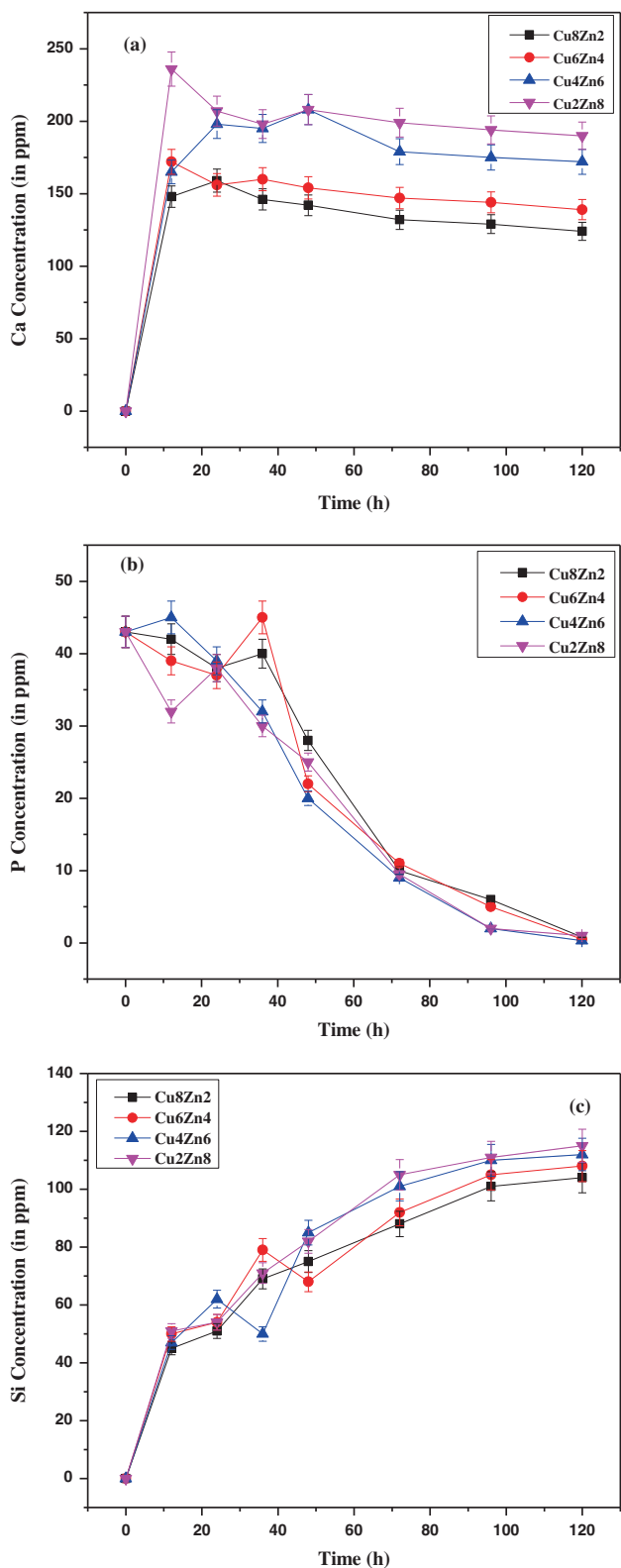


Fig. 3 a Ca, b P and c Si concentration in SBF as function of time for all glass samples

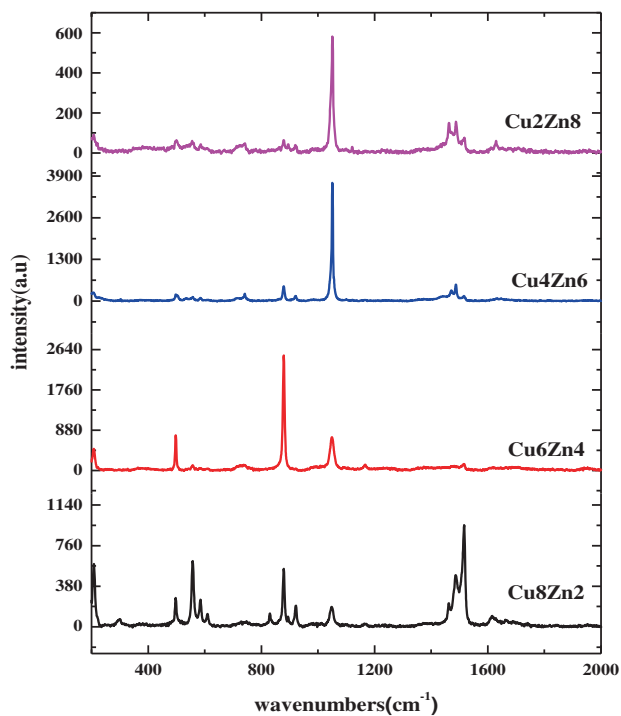


Fig. 4 Spectra of Raman analysis of glass samples Cu₈Zn₂, Cu₆Zn₄, Cu₄Zn₆ and Cu₂Zn₈

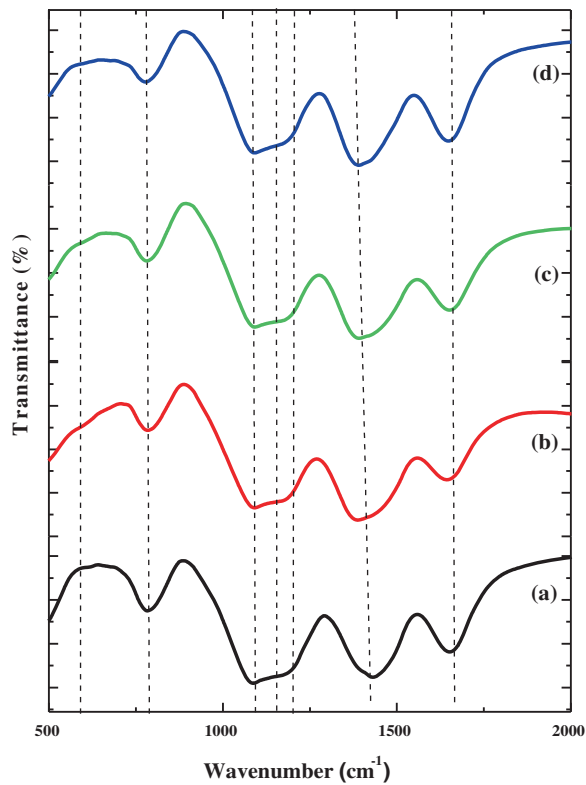


Fig. 5 FT-IR spectrum of glass samples a Cu₈Zn₂, b Cu₆Zn₄, c Cu₄Zn₆ and d Cu₂Zn₈

Table 4 Groups corresponding to different wavenumbers for the present compositions [8]

Wavenumber (cm ⁻¹)	Group
550–590	Si–O–Si bending
740–760	P–O–P stretching
1110–1125	Si–O–Si antisymmetric stretching
1200–1220	P=O stretching
1420–1440	H ₂ O and hydrogen bonding
1610–1630	H ₂ O and hydrogen bonding

The loading of these drugs in MBGs Cu₈Zn₂, Cu₆Zn₄, Cu₄Zn₆ and Cu₂Zn₈ is shown in Figs. 7–10 respectively. The loading kinetics of VANCO, DOX and TETRA for all the MBGs are given in Figs. 11–13, respectively. The amount of drug loaded in the MBGs is given in Tables 5 and 6.

3.8 Vibrating sample magnetometer

MBGs were characterized further to know about its magnetic behavior when exposed to the magnetic field. The hysteresis loop of Cu₈Zn₂, Cu₆Zn₄, Cu₄Zn₆ and Cu₂Zn₈ MBGs are shown in Fig. 14a–d, respectively. The hysteresis loop is obtained from the characterization of different glass samples at room temperature.

4 Discussions

All the as prepared glasses exhibit halo peaks in between 12–15° hence confirming their amorphous nature (Fig. 1). All the glasses show long-range structural disorder with a small hump around 27°, which is also reported by Kaur et al. [8] for the copper containing glasses. Molar mass of the samples increased with increasing zinc and decreasing copper content and varies as Cu₈Zn₂<Cu₆Zn₄<Cu₄Zn₆<Cu₂Zn₈ (Table 2). Moreover, molar volume of these glass samples varies from 38.53 to 46.61 cm³/mol as the copper content decreasing in MBGs. Molar volume of the samples showed decreasing trend with decreasing copper content, however for Cu₂Zn₈ MBG, V_m increased and reached the value 46.02 cm³/mol. In addition to this, density of MBGs varied from 1.40 to 1.72 g/cm³ with increasing zinc content. Density of MBGs showed an increasing trend with decreasing copper content, however for Cu₂Zn₈ MBG, density value decreased and reached 1.44 g/cm³. In addition to this, specific surface area of samples also increased from 263 to 402 cm²/g with increasing zinc content. As the copper content decreases in MBGs, pore volume increases from 0.77 to 0.93 cm³/g. The results obtained by different research groups for pore size values yield an optimized value of mesopores between 2–50 nm, approximately [2, 13–15].

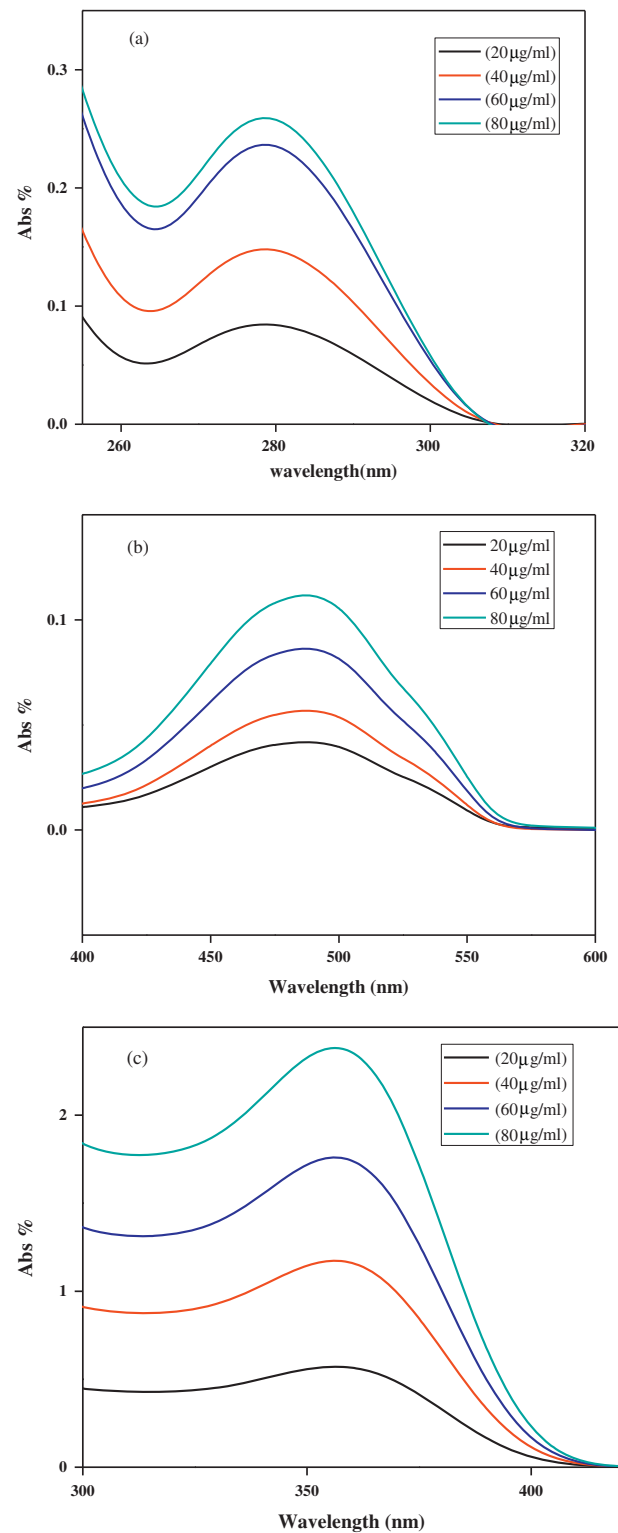
**Fig. 6** Calibration curves of **a** VANCO, **b** DOX and **c** TETRA respectively

Figure 2a–d indicates that apatite layer increases as the zinc concentration increases in the MBGs. For MBG with highest zinc content, i.e. Cu₂Zn₈, the apatite layer density is

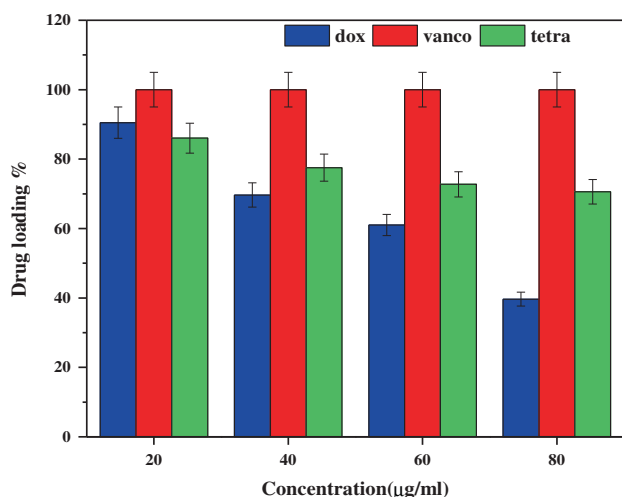


Fig. 7 Drug loading capability of glass sample Cu8Zn2 for VANCO, DOX and TETRA drugs at different concentrations

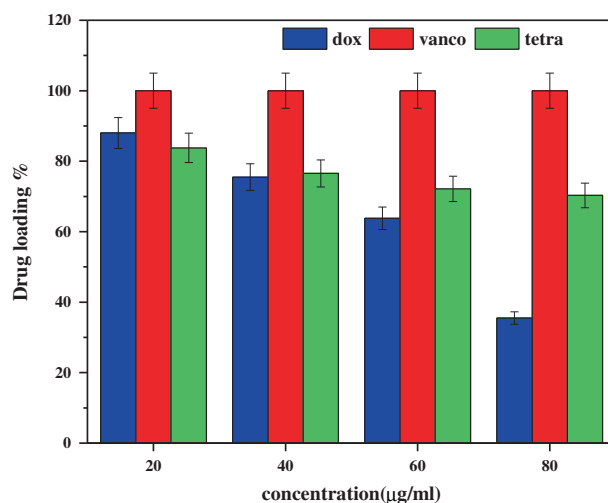


Fig. 9 Drug loading capability of glass sample Cu4Zn6 for VANCO, DOX and TETRA drugs at different concentrations

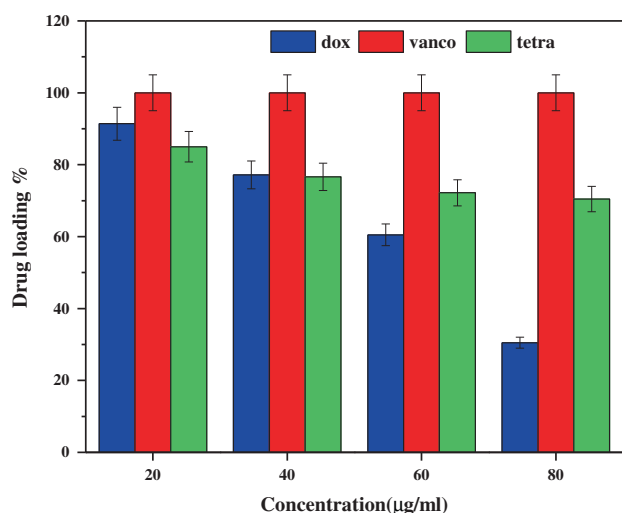


Fig. 8 Drug loading capability of glass sample Cu6Zn4 for VANCO, DOX and TETRA drugs at different concentrations

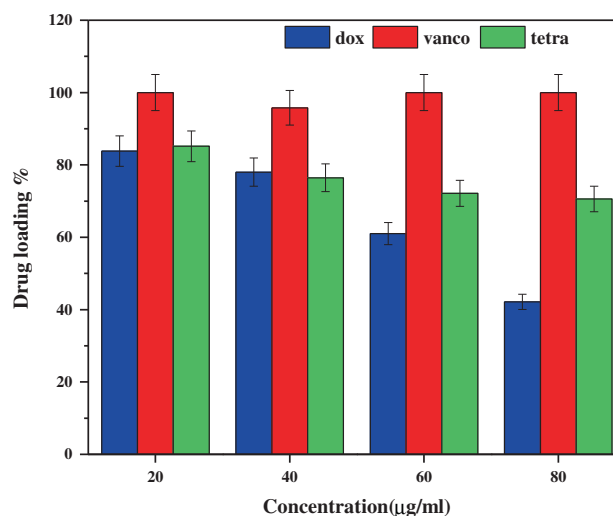


Fig. 10 Drug loading capability of glass sample Cu2Zn8 for VANCO, DOX and TETRA drugs at different concentrations

higher. Rough and porous structure for all the MBGs could be seen, particularly for the Cu2Zn8. Therefore, it indicates rapid degradation kinetics and apatite formation for Cu2Zn8 MBG as compared to other MBGs. Figure 3a indicates that the stabilization of Ca concentration in Cu8Zn2 and Cu6Zn4 MBGs arrive earlier than other MBGs. It was observed that, samples with low content of copper release higher Ca to the SBF solution. The Ca concentration profile follows the trend as Cu2Zn8 > Cu4Zn6 > Cu6Zn4 > Cu8Zn2. After 48 h of soaking in SBF solution, all the MBGs show decrease in P concentration (Fig. 3b). After 72 h of soaking, all the MBGs reveal almost stable concentration for Si (Fig. 3c).

The Raman spectra (Fig. 4) depicts that the silica Si-O_b-Si peaks in 450–550 cm⁻¹ region, are more prominent for Cu6Zn4 and Cu8Zn2 MBGs, as compared to other two MBGs. Si-O_{nb} (nb—non-bridging) peak between 1000–1050 cm⁻¹ range are more prominent for Cu4Zn6 and Cu2Zn8 MBGs glass samples. Raman spectra indicates that among all the glass samples, Cu8Zn2 MBG shows maximum number of peaks as compared to other glass samples, so it is concluded that glass sample with high copper contents is highly Raman active.

From the FTIR spectra as shown in Fig. 5, peak at position 550–590 cm⁻¹ represents Si-O-Si bending whereas peak at 740–760 cm⁻¹ represents the presence of P-O-P stretching. In addition to this, prominent peak of silicate

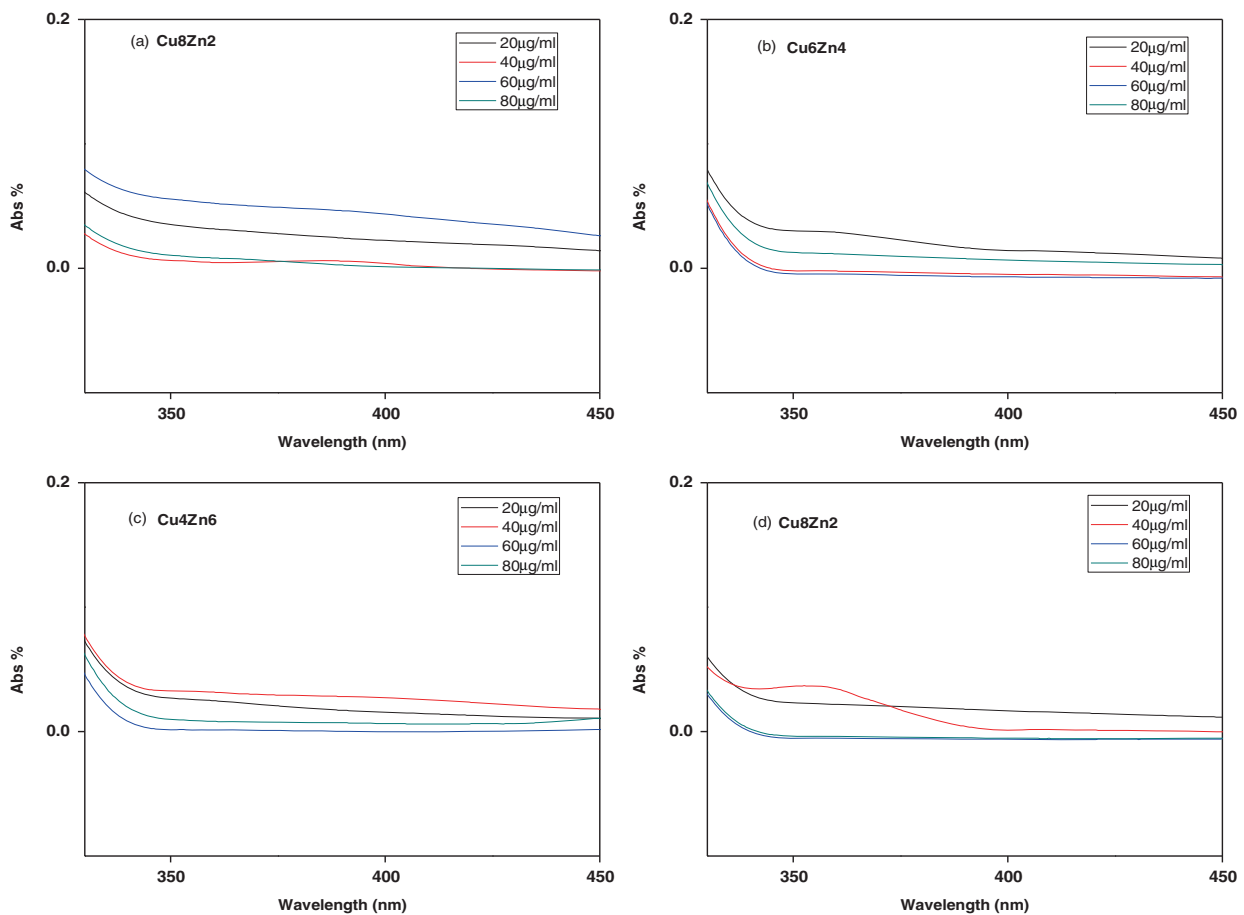


Fig. 11 Loading of VANCO in **a** Cu₈Zn₂, **b** Cu₆Zn₄, **c** Cu₄Zn₆ and **d** Cu₂Zn₈ mesoporous glasses respectively at different concentrations

band Si-O-Si anti-symmetric stretching is observed at 1110–1125 cm^{-1} . Furthermore, a stretching peak of P=O is observed for 1200–1220 cm^{-1} range. These peaks represent the presence of high amount of silica and phosphorous in MBGs [51–53]. An increase in pH and silica formation layer is observed leading to precipitation of CaO–P₂O₅ rich layer followed by the occurrence of crystallization causing to form apatite layer. The bands observed at greater than 1400 cm^{-1} represent the presence of H₂O molecules, OH⁻ and hydrogen bonding.

For loading, the channels of mesoporous glasses play a vital role. The drug is injected in MBGs or is incorporated in the mesopores of the glass by soaking the MBG into drug-ddH₂O solution, where drug lies in the pores of the glasses along with a small fraction on the external surface. Also, portions of drug exist on the pore opening windows of the channels. However, greater fraction of drug lies inside the pores of the mesoporous glass. Pore size and pore volume plays important role in the loading kinetics. Pores are filled with drug when drug mesopore interaction occurs, even though this interaction is a surface phenomenon [8, 15–19].

In the present study, three drugs namely VANCO, DOX and TETRA have been loaded individually in the mesoporous glass matrix. These are loaded at different concentrations at 20, 40, 60 and 80 $\mu\text{g/ml}$ in ultrapure distilled water. The amount of drugs loaded in the mesoporous glasses is obtained from the calibration curves.

It was observed that when VANCO is loaded in Cu₈Zn₂, it was fully loaded at all concentrations. However, DOX and TETRA had highest loading on 20 $\mu\text{g/ml}$ for all the glasses. With increasing concentration of drug and decreasing copper content, loading was decreased from 90.5 to 39.67% in case of DOX, while for TETRA, it was decreased from 85 to 70.44%. In all glass samples, VANCO drug is loaded completely except for Cu₂Zn₈ at 40 $\mu\text{g/ml}$ (95%). However, DOX and TETRA drugs loading decreased with decreasing copper content and increased drug concentrations.

For the present MBGs, it is found that the VANCO is fully loaded in almost all glass samples at all concentrations as shown in Fig. 11a–d. Anyhow, for Cu₂Zn₈ glass, at concentration 40 $\mu\text{g/ml}$, 95.78% drug was loaded, otherwise, for glass samples Cu₈Zn₂, Cu₆Zn₄ and Cu₄Zn₆, the

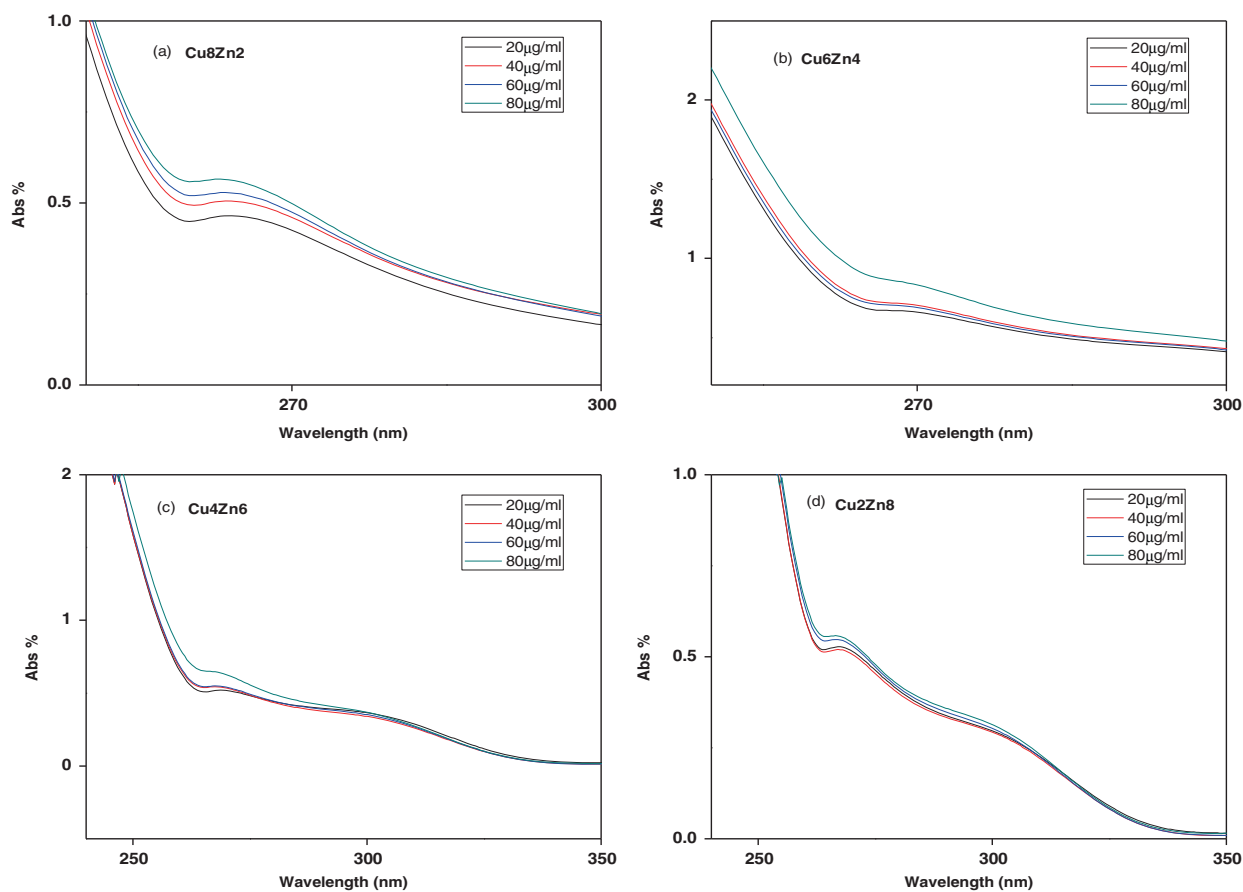


Fig. 12 Loading of DOX in **a** Cu8Zn2, **b** Cu6Zn4, **c** Cu4Zn6 and **d** Cu2Zn8 mesoporous glasses respectively at different concentrations

drug is fully loaded, that is, 100% for all concentrations (20, 40, 60 and 80 µg/ml). Even for glass sample Cu2Zn8, at concentrations 20, 60 and 80 µg/ml, the drug is loaded 100%. It is estimated from this result that MBGs with decreasing copper and increasing zinc content are a considerable drug carrier for the VANCO drug. Dion et al. [54] studied the vancomycin release from amorphous calcium polyphosphate matrices. Authors had studied the loaded vancomycin for different time periods (0, 5 and 24 h) in the gelled spheres. The loading of the vancomycin had decreased as the loading duration was increased and loading order of the drug is 72, 68 and 60% for 0, 5 and 24 h, respectively.

For the DOX, as the drug concentration and zinc content is increased, loading decreases as shown in Fig. 12a–d. For instance, at concentration of 20 µg/ml, for Cu8Zn2 glass sample, loading is obtained to be 90.5%. However for the same glass sample, when drug concentration reached 80 µg/ml, loading decreases to 39.67%. Similarly, for all other glass samples at different concentrations, loading of drugs varied. For Cu6Zn4 glass sample, loading was decreased from 91.4 to 30.5% with increasing concentrations of the drug. For Cu4Zn6 glass sample, loading decreased from 88

to 35.5% and also for Cu8Zn2 glass sample, loading decreased up to 42.17 from 83.83%. The loading percentage of VANCO, DOX and TETRA is shown in Tables 5 and 6. Wu et al. [48] obtained 90% loading for DOX when MBG nanospheres were dissolved in DOX + phosphate buffered saline (PBS). It was concluded that, when concentration of DOX was increased, loading of MBG nanospheres also increased. The loading of MBG nanospheres reached 31.46 mg/g with the highest concentration of drug.

Similarly as DOX, loading of TETRA also decreased with increased drug concentration as shown in Fig. 13a–d. But unlike DOX, loading of TETRA decreased considerably low with decreasing copper content or increasing zinc content. In glass sample Cu8Zn2, loading decreased from 86.04 to 70.6% with increasing the drug concentration. For glass sample Cu6Zn4 sample, loading was from 85 to 70.44% with increasing concentration. For Cu4Zn6 and Cu2Zn8, loading obtained decreased from 83.78 to 70.29% and 85.16 to 70.6% respectively. Domingues et al. [55] studied the in vivo biocompatibility, physical-chemical properties and antimicrobial activity of bioactive glass (BG) loaded with tetracycline and its inclusion complex β -cyclodextrin. Authors had obtained 73% loading efficiency

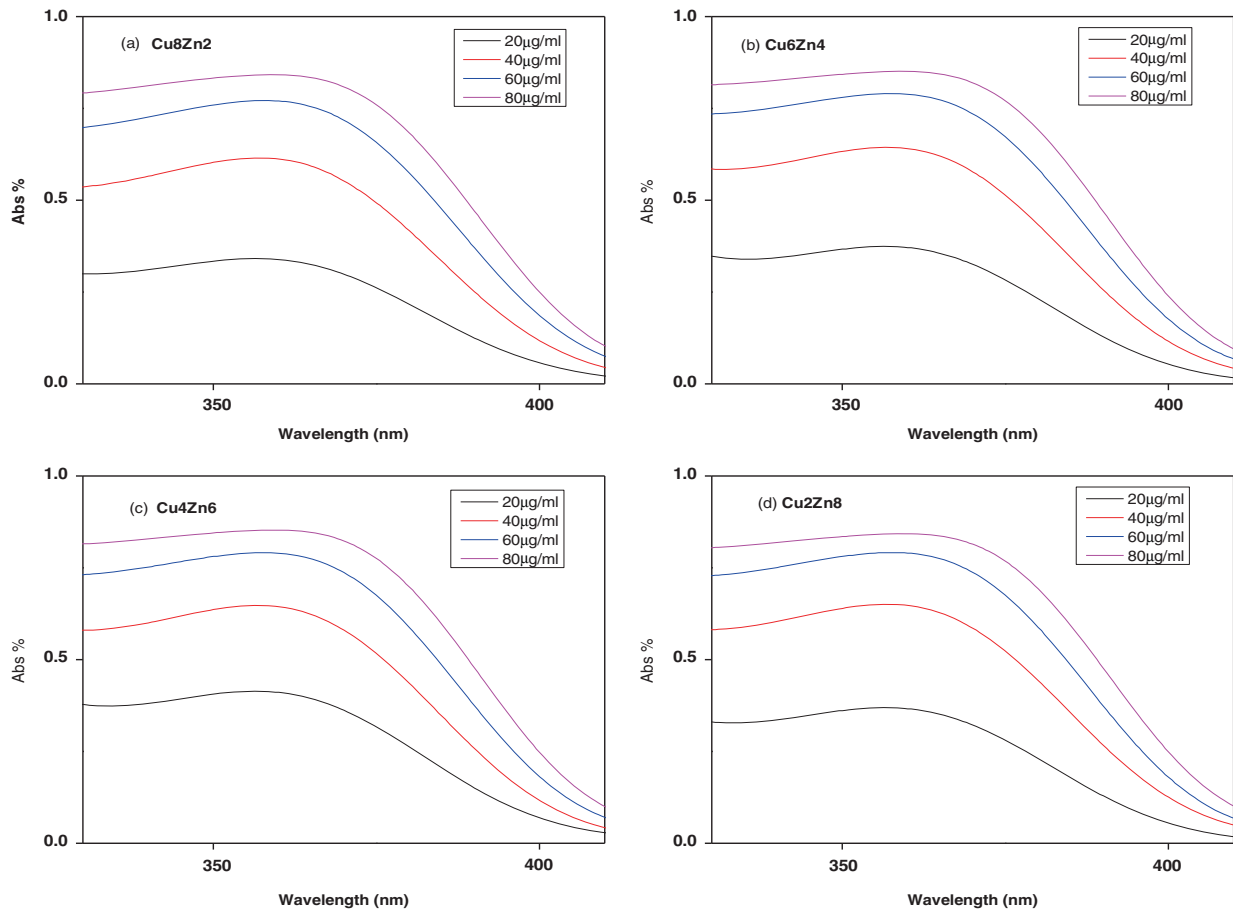


Fig. 13 Loading of TETRA in **a** Cu8Zn2, **b** Cu6Zn4, **c** Cu4Zn6 and **d** Cu2Zn8 mesoporous glasses respectively at different concentrations

Table 5 Drug loading capability (in %) of glass samples Cu8Zn2 and Cu6Zn4 for VANCO, DOX and TETRACYCLINE drugs at different concentrations

Drug concentration (µg/ml)	Cu8Zn2			Cu6Zn4		
	VANCO	DOX	TETRA	VANCO	DOX	TETRA
20	100	90.5	86.04	100	91.4	85
40	100	69.67	77.54	100	77.17	76.63
60	100	61	72.75	100	60.5	72.19
80	100	39.67	70.6	100	30.5	70.44

Table 6 Drug loading capability (in %) of glass samples Cu4Zn6 and Cu2Zn8 for VANCO, DOX and TETRACYCLINE drugs at different concentrations

Drug concentration (µg/ml)	Cu4Zn6			Cu2Zn8		
	VANCO	DOX	TETRA	VANCO	DOX	TETRA
20	100	88	83.78	100	83.83	85.16
40	100	75.5	76.54	95.78	78	76.44
60	100	63.83	72.16	100	61	72.13
80	100	35.5	70.29	100	42.17	70.6

of tetracycline in bioactive glass. The highest loading that our group obtained for tetracycline is reported to be 86.04% implying that the MBGs are more considerable candidates for drug loading as compared to BGs.

The magnetization results showed that the area of magnetization is very less as evident from Fig. 14a–d. Hence, the small area of magnetization indicates that as prepared samples are soft magnetic in nature. Copper and zinc both

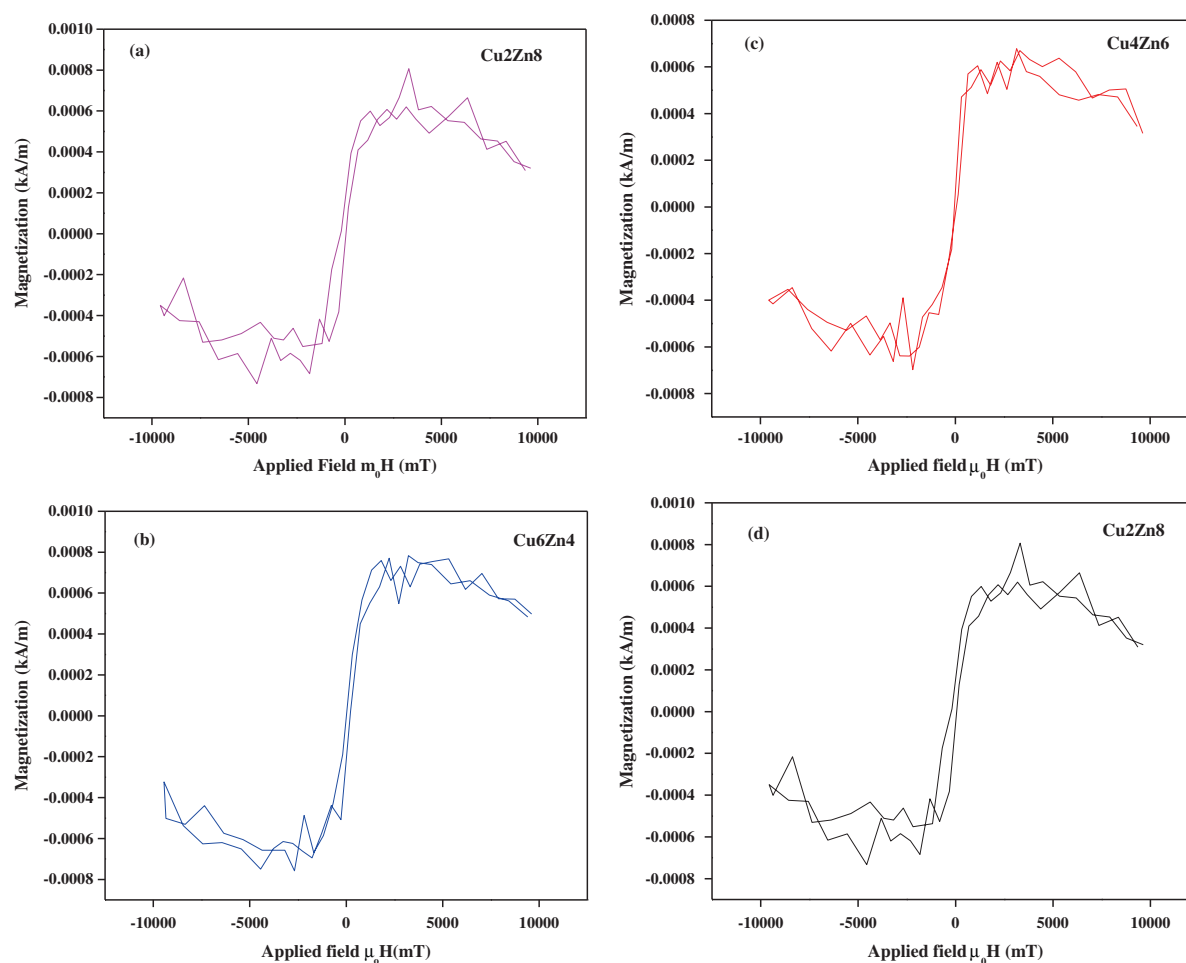


Fig. 14 Magnetic behavior of samples **a** Cu8Zn2, **b** Cu6Zn4, **c** Cu4Zn6 and **d** Cu2Zn8

are diamagnetic elements, so these do not show very strong magnetic behavior. Therefore, in the present study of VSM, no influential results could be obtained.

5 Conclusions

In present study, the mesoporous bioactive glass (MBG) series composed of $(10-x)\text{CuO}-x\text{ZnO}-20\text{CaO}-60\text{SiO}_2-10\text{P}_2\text{O}_5$ were fabricated using CTAB as structure directing agent. The antibacterial and anticancerous drugs were loaded in the fabricated glasses and their drug loading efficiency was checked. The drugs loaded in MBG were doxorubicin (anticancerous), vancomycin and tetracycline (antibacterial). The MBGs yielded pore size in the acceptable range of 4–10 nm. The MBGs have porous and rough structure and formation of apatite layer on their surfaces. Furthermore, the MBGs yielded most prominent bands at $1110\text{--}1125\text{ cm}^{-1}$ attributed to Si-O-Si anti-symmetric stretching. Apart from this, VSM showed the soft

magnetic nature for the MBGs. Drug loading kinetics revealed the highest loading of VANCO (100%) for all glass samples. Decrease in the loading of DOX and TETRA with decreasing copper content and increasing drug concentration was observed. The decreasing copper content affected the loading of two drugs Doxorubicin (DOX) and Tetracycline (TETRA), whereas Vancomycin (VANCO) remained unaffected of the decreasing copper content or increasing zinc content in the glass samples.

Acknowledgment One of the author, GK is thankful to University Grant Commission (UGC) under the letter no.—F.15/2013-2014/PDFWM-2013-2014-GE-PUN-14803 (SA-II) for providing financial assistance.

Compliance with ethical standards

Conflict of interest The authors declare that they have no competing interests.

References

- Kaur G, Pickrell G, Sriranganathan N, Kumar V, Homa D. Review and the state of the art: sol-gel and melt quenched bioactive glasses for tissue engineering. *J Biomed Mater Res B*. 2015;104:1248–75.
- Kaur G, Pandey OP, Singh K, Homa D, Scott B, Pickrell G. A review of Bioactive glasses: their structure, properties, fabrication and apatite formation. *J Biomed Mater Res A*. 2014;102(1):254–74.
- Li HC, Wang DG, Hu JH, Chen CZ. Crystallization, mechanical properties and in vitro bioactivity of sol-gel derived $\text{Na}_2\text{O}-\text{CaO}-\text{SiO}_2-\text{P}_2\text{O}_5$ glass-ceramics by partial substitution of CaF_2 for CaO . *J Sol Gel Sci Technol*. 2013;67:56–65.
- AJA PN, AJA AH, PENA P and AJA S. Bioactive glasses and glass ceramics. *Bol Soc Esp Ceram Vid*. 2007;46(2):45–55.
- Hum J, Boccaccini A R. Bioactive glasses as carriers for bioactive molecules and therapeutic drugs: a review. *J Mater Sci*. 2012; 23(10):2317–33.
- Rahaman MN, Day DE, Bal BS, Fu Q, Jung SB, Bonewald LF, Tomsia AP. Bioactive glass in tissue engineering. *Acta Biomater*. 2011;7:2355–73.
- Du RL, Chang J, Ni SY, Zhai WY. Characterization and in vitro bioactivity of zinc-containing bioactive glass and glassceramics. *J Biomater Appl*. 2006;20:341–60.
- Kaur G, Pandey OP, Singh K, Chudasama B, Kumar V. Combined and individual doxorubicin/vancomycin drug loading, release kinetics and apatite formation for the $\text{CaO}-\text{CuO}-\text{P}_2\text{O}_5-\text{SiO}_2-\text{B}_2\text{O}_3$ mesoporous glasses. *RSC*. 2016;6:51046–56.
- Goel A, Kapoor S, Tilocca A, Rajagopal RR, Ferreira JMF. Structural role of zinc in biodegradation of alkali-free bioactive glasses. *J Mater Chem B*. 2013;1:3073–82.
- Venkatesan J, Pallela R, Bhatnagar I, Kim SK. Chitosan-amylopectin/hydroxyapatite and chitosan-chondroitin sulphate/hydroxyapatite composite scaffolds for bone tissue engineering. *Int J Biol Macromol*. 2012;51:1033–42.
- Xia W, Chang J. Well-ordered mesoporous bioactive glasses (MBG): a promising bioactive drug delivery system. *J Control Release*. 2006;110:522–30.
- Noriega AL, Arcos D, Barba II, Sakamoto Y, Terasaki O, Regi MV. Ordered mesoporous bioactive glasses for bone tissue regeneration. *Chem Mater*. 2006;18:3137–44.
- Wu C, Zhang Y, Zhu Y, Friis T, Xiao Y. Structure–property relationships of silk-modified mesoporous bioglass scaffolds. *Biomaterials*. 2010;31:3429–38.
- Wu C, Fan W, Gelinsky M, Xiao Y, Simon P, Schulze R, Doert T, Luo Y, Cuniberti G. Bioactive $\text{SrO}-\text{SiO}_2$ glass with well-ordered mesopores: characterization, physiochemistry and biological properties. *Acta Biomater*. 2011;7:1797–806.
- Regi MV, Balas F, Arcos D. Mesoporous materials for drug delivery. *Angew Chem Int Ed*. 2007;46:7548–58.
- Torchilin VP. Recent advances with liposomes as pharmaceutical carriers. *Nat Rev Drug Discov*. 2005;4:145–60.
- Yoo W, Lee CH. Drug delivery system for hormone. *J Control Release*. 2006;112:1–14.
- Malmsten M. Soft drug delivery system. *Soft Mater*. 2006; 2:760–9.
- Regi MV. Ordered mesoporous materials in the context of drug delivery systems and bone tissue engineering. *Chem Eur J*. 2006;12:5934–43.
- Regi MV, Ramila A, Real RP. A new property of MCM-41: drug delivery system. *J Perez-Pariente Chem Mater*. 2001;13:308–311.
- Fournier E, Passirani C, Montero-Menei CN, Benoit JP. Biocompatibility of implantable synthetic polymer drug carriers: focus on brain biocompatibility. *Biomater*. 2003;24:3311–31.
- Day RM, Boccaccini AR, Shurey S, Roether JA, Forbes A, Hench LL, Gabe SM. Assessment of polyglycolic acid mesh and bioactive glass for soft-tissue engineering scaffolds. *Biomaterials*. 2004;25:5857–66.
- Day RM. Bioactive glass stimulates the secretion of angiogenic growth factors and angiogenesis in vitro. *Tissue Eng*. 2005; 11:768–77.
- Gorustovich AA, Roether JA, Boccaccini AR. Effect of bioactive glasses on angiogenesis: a review of in vitro and in vivo evidences. *Tissue Eng Part B Rev*. 2009;16:199–207.
- Leu A, Stieger SM, Dayton P, Ferrara KW, Leach JK. Angiogenic response to bioactive glass promotes bone healing in an irradiated calvarial defect. *Tissue Eng Part A*. 2009;15:877–85.
- Jones JR, Ehrenfried LM, Hench LL. Optimising bioactive glass scaffolds for bone tissue engineering. *Biomaterials*. 2006;27:964–73.
- Liu H, Webster TJ. Nanomedicine for implants: a review of studies and necessary experimental tools. *Biomaterials*. 2007; 28:354–69.
- Wu C, Chang J. Mesoporous bioactive glasses: structure characteristics, drug/growth factor delivery and bone regeneration application. *Interface Focus*. 2012;2:292–306.
- Li Y, Liu YZ, Long T, Yu XB, Tang TT, Dai KR, Tian B, Guo YP, Zhu ZA. Mesoporous bioactive glass as a drug delivery system: fabrication, bactericidal properties and biocompatibility. *J Mater Sci*. 2013;24:1951–61.
- Lu H, Kawazoe N, Kitajima T, Myoken Y, Tomita M, Umezawa A, Chen G, Ito Y. Spatial immobilization of bone morphogenetic protein-4 in a collagen-PLGA hybrid scaffold for enhanced osteoinductivity. *Biomaterials*. 2012;33:6140–6.
- Liu X, Rahaman MN, Fu Q. Bone regeneration in strong porous bioactive glass (13–93) scaffolds with an oriented microstructure implanted in rat calvarial defects. *Acta Biomater*. 2013;9:4889–98.
- Nguyen TH, Lee BT. In vitro and in vivo studies of rhBMP2-coated PS/PCL fibrous scaffolds for bone regeneration. *J Biomed Mater Res A*. 2013;101:797–808.
- Wu C, Zhou Y, Xu M, Han P, Chen L, Chang J, Xiao Y. Copper-containing mesoporous bioactive glass scaffolds with multifunctional properties of angiogenesis capacity, osteostimulation and antibacterial activity. *Biomater*. 2013;34:422–33.
- Park JK, Shim JH, Kang KS, Yeom J, Jung HS, Kim JY, et al. Solid free-form fabrication of tissue-engineering scaffolds with a poly(lactic-co-glycolic acid) grafted hyaluronic acid conjugate encapsulating an intact bone morphogenetic protein-2/poly(ethylene glycol) complex. *Adv Funct Mater*. 2011;21:2906–12.
- Baino F, Fiorilli S, Brovarone CV. Bioactive glass-based materials with hierarchical porosity for medical applications: Review of recent advances. *Acta Biomater*. 2016;42:18–32.
- Wu C, Chang J. Multifunctional mesoporous bioactive glasses for effective delivery of therapeutic ions and drug/growth factors. *J Control Release*. 2014;193:282–95.
- Hench LL, Thompson I. Twenty-first century challenges for biomaterials. *J R Soc Interface*. 2010;7(4):S379–91.
- Wu C, Zhou Y, Xu M, Han P, Chen L, Chang J, Xiao Y. Copper-containing mesoporous bioactive glass scaffolds with multifunctional properties of angiogenesis capacity, osteostimulation and antibacterial activity. *Biomater*. 2013;34:422–33.
- Kim TG, Shin H, Lim DW. Biomimetic scaffolds for tissue engineering. *Adv Funct Mater*. 2012;22:2446–68.
- Wang C, Xue Y, Lin K, Lu J, Chang J, Sun J. The enhancement of bone regeneration by a combination of osteoconductivity and osteostimulation using $\beta\text{-CaSiO}_3/\beta\text{-Ca}_3(\text{PO}_4)_2$ composite bioceramics. *Acta Biomater*. 2012;8:350–360.
- Hu YC, Zhong JP. Osteostimulation of bioglass. *Chin Med J (Engl)*. 2009;122:2386–9.
- Freeman AL, MD and Mayhew E. Targeted Drug Deliv. *Cancer*. 1986;58:573–83.

43. McCarthy TJ, Zeelie JJ, Krause DJ. The antimicrobial action of zinc ion/antioxidant combinations. *J Clin Pharm Ther.* 1992;17:51–54.
44. Solomons NW. Mild human zinc deficiency produces an imbalance between cell-mediated and humoral immunity. *Nutr Rev.* 1998;56:27–28.
45. Prasad AS. Zinc: an overview. *Nutrition.* 1995;11:93–9.
46. Harris ED. Copper homeostasis: the role of cellular transporters. *Nutr Rev.* 2001;59:281–5.
47. Tas AC. Synthesis of biomimetic Ca-hydroxyapatite powders at 37°C in synthetic body fluids. *Biomater.* 2000;21:1429–38.
48. Wu HC, Wang TW, Sun JS, Wang WH, Lin FH. A novel bi-magnetic nanoparticle based on hydroxyapatite. *Nanotechnology.* 2007;18:1–9.
49. Marsich L, Moimas L, Sergio V, Schmid C. Raman spectroscopic study of bioactive silica-based glasses: the role of alkali/alkali earth ratio on the non-bridging oxygen/bridging oxygen (NBO/BO) ratio. *Spectroscopy.* 2009;23(3–4):227–232.
50. Pemberton JE, Latifzadeh L, Fletcher JP, Risbud SH. Raman spectroscopy of calcium phosphate glasses with varying CaO modifier concentrations. *Chem Mater* 1991;3(1):195–200.
51. Kaur G, Pickrell G, Kimsawatde G, Homa D, Allbee HA, Sriranganathan N. Synthesis, cytotoxicity, and hydroxyapatite formation in 27-tris-SBF for sol-gel based CaO–P₂O₅–SiO₂–B₂O₃–ZnO bioactive glasses. *Sci Rep.* 2014;4:1–14.
52. Kaur G, Sharma P, Kumar V, Singh K. Assessment of in vitro bioactivity of SiO₂–BaO–ZnO–B₂O₃–Al₂O₃ glasses: an optico-analytical approach. *Mater Sci Eng,C.* 2012;32:1941–7.
53. Kaur G, Kumar M, Arora A, Pandey OP, Singh K. Influence of Y₂O₃ on structural and optical properties of SiO₂–BaO–ZnO–xB₂O₃–(10–x)Y₂O₃ glasses and glass ceramics. *J Non Cryst Solids.* 2011;357:858–63.
54. Dion A, Langman M, Hall G, Filiaggi M. Vancomycin release behaviour from amorphous calcium polyphosphate matrices intended for osteomyelitis treatment. *Biomater.* 2005;26:7276–85.
55. Domingues ZR, Cortès ME, Gomes TA, Diniz HF, Freitas CS, Gomes JB, Faria AMC, Sinisterra RD. Bioactive glass as a drug delivery system of tetracycline and tetracycline associated with β-cyclodextrin. *Biomaterials.* 2004;25(2):327–33.